

Direct visualization of structural defects in 2D semiconductors

Yutuo Guo(郭玉拓)1,2, Qinqin Wang(王琴琴)1,2, Xiaomei Li(李晓梅)1,2, Zheng Wei(魏争)1,2, Lu Li(李璐)1,2, Yalin Peng(彭雅琳)1,2, Wei Yang(杨威)1,2, Rong Yang(杨蓉)1,2,3, Dongxia Shi(时东霞)1,2, Xuedong Bai(白雪冬)1,2, Luojun Du(杜罗军)1,2, and Guangyu Zhang(张广宇)1,2,3,†

Citation: Chin. Phys. B, 2022, 31 (7): 076105 DOI: 10.1088/1674-1056/ /ac6738
Journal homepage: http://cpb.iphy.ac.cn; http://iopscience.iop.org/cpb

What follows is a list of articles you may be interested in

Evolution of defects and deformation mechanisms in different tensile directions of solidified lamellar Ti-Al alloy

Yutao Liu(刘玉涛), Tinghong Gao(高廷红), Yue Gao(高越), Lianxin Li(李连欣), Min Tan(谭敏), Quan Xie(谢泉), Qian Chen(陈茜), Zean Tian(田泽安), Yongchao Liang(梁永超), and Bei Wang(王蓓)

Chin. Phys. B, 2022, 31 (**4**): 046105. DOI: 10.1088/1674-1056/ac1f0b

Dislocation slip behaviors in high-quality bulk GaN investigated by nanoindentation

Kai-Heng Shao(邵凯恒), Yu-Min Zhang(张育民), Jian-Feng Wang(王建峰), and Ke Xu(徐科)

Chin. Phys. B, 2021, 30 (**11**): 116104. DOI: 10.1088/1674-1056/abfd9e

Polycrystalline cubic boron nitride prepared with cubic-hexagonal boron nitride under high pressure and high temperature

Ming Yang(杨鸣), Zi-Li Kou(寇自力), Teng Liu(刘腾), Jing-Rui Lu(卢景瑞), Fang-Ming Liu(刘方明), Yin-Juan Liu(刘银娟), Lei Qi(戚磊), Wei Ding(丁未), Hong-Xia Gong(龚红霞), Xiao-Lin Ni(倪小林), Duan-Wei He(贺端威)

Chin. Phys. B, 2018, 27 (**5**): 056105. DOI: 10.1088/1674-1056/27/5/056105

Facile and controllable synthesis of molybdenum disulfide quantum dots for highly sensitive and selective sensing of copper ions

Xue Li(李雪), Da-Wei He(何大伟), Yong-Sheng Wang(王永生), Yin Hu(胡音), Xuan Zhao(赵宣), Chen Fu(付晨), Jing-Yan Wu(吴静燕)

Chin. Phys. B, 2018, 27 (**5**): 056104. DOI: 10.1088/1674-1056/27/5/056104

Electric field modulation technique for high-voltage AlGaN/GaN Schottky barrier diodes

Tang Cen, Xie Gang, Zhang Li, Guo Qing, Wang Tao, Sheng Kuang

Chin. Phys. B, 2013, 22 (**10**): 106107. DOI: 10.1088/1674-1056/22/10/106107

RAPID COMMUNICATION

Direct visualization of structural defects in 2D semiconductors

Yutuo Guo(郭玉拓)[1,2], Qinqin Wang(王琴琴)[1,2], Xiaomei Li(李晓梅)[1,2], Zheng Wei(魏争)[1,2], Lu Li(李璐)[1,2], Yalin Peng(彭雅琳)[1,2], Wei Yang(杨威)[1,2], Rong Yang(杨蓉)[1,2,3], Dongxia Shi(时东霞)[1,2], Xuedong Bai(白雪冬)[1,2], Luojun Du(杜罗军)[1,2], and Guangyu Zhang(张广宇)[1,2,3,†]

[1] *Beijing National Laboratory for Condensed Matter Physics and Institute of Physics, Chinese Academy of Sciences, Beijing* 100190, *China*
[2] *School of Physical Science, University of Chinese Academy of Sciences, Beijing* 100049, *China*
[3] *Songshan-Lake Materials Laboratory, Dongguan* 523808, *Guangdong Province, China*

(Received 15 March 2022; revised manuscript received 6 April 2022; accepted manuscript online 14 April 2022)

Direct visualization of the structural defects in two-dimensional (2D) semiconductors at a large scale plays a significant role in understanding their electrical/optical/magnetic properties, but is challenging. Although traditional atomic resolution imaging techniques, such as transmission electron microscopy and scanning tunneling microscopy, can directly image the structural defects, they provide only local-scale information and require complex setups. Here, we develop a simple, non-invasive wet etching method to directly visualize the structural defects in 2D semiconductors at a large scale, including both point defects and grain boundaries. Utilizing this method, we extract successfully the defects density in several different types of monolayer molybdenum disulfide samples, providing key insights into the device functions. Furthermore, the etching method we developed is anisotropic and tunable, opening up opportunities to obtain exotic edge states on demand.

Keywords: structural defects, direct visualization, molybdenum disulfide, anisotropic etching, edges

PACS: 61.72.Ff, 68.65.–k **DOI:** 10.1088/1674-1056/ac6738

1. Introduction

Structural defects in two-dimensional (2D) semiconductors, such as zero-dimensional (0D) point defects and one-dimensional (1D) grain boundaries, play important roles on modulation of their mechanical, electrical, optical, and chemical properties.[1–6] For examples, the vacancies and grain boundaries in 2D transition metal dichalcogenides (TMDs) can offer effective catalytic active sites and thus enhance the catalytic performance.[7–9] On the other hand, structural defects usually act as additional scattering centers and degrade the electric performance, such as mobility and on/off ratio.[2,6,10,11] As a consequence, it is essential to know the details of structural defects in 2D semiconductors on a large scale, such as the density and the location, which can provide key information to deeply understand their properties and to guide the further optimization.

Arguably the atomic resolution microscopy tools, such as high-resolution transmission electron microscopy (HRTEM) and scanning tunneling microscopy (STM),[12–15] can directly visualize the structural defects in 2D semiconductors. However, these atomic resolution techniques not only cannot give large-scale information (usually only a few tens of nanometers), but also require ultra-high vacuum, complex setups or specialized sample preparation, making them impractical to be a usual basis to characterize structural defects in 2D semiconductors. Remarkably, because of the high reactivity, atomic-scale structural defects can be enlarged into macroscopic structures after being etched, offering the possibility for direct visualization on a large scale through atomic force microscope (AFM) or even optical microscope.[16–18] Recently, multiple methods have been developed to directly image the structural defects in 2D semiconductors on a large scale, for example, via enlarging the defect sites by selective etching or decorating them with nanoparticles.[18–20] However, these methods either introduce new defects or lead to surface modifications.[2,9,16,19,21–29] Damage to the surface and quality of 2D semiconductors hinders their further applications.

In this paper, we introduce a non-invasive, facile method for large-scale assessment of structural defects in monolayer molybdenum disulfide (ML-MoS_2), a prototypical 2D semiconductor. Weak wet etching is utilized to enlarge those structural defects in ML-MoS_2 for direct visualization under optical microscope or AFM. The weak etching only etches the defected sites while keeping the perfect lattice of ML-MoS_2 intact, as confirmed by TEM, AFM and photoluminescence (PL) spectroscopy. Using this technique, we systematically investigated the defects in different types of ML-MoS_2 samples, providing key information to understand their electrical performance.

2. Methods

2.1. Sample fabrications

All monolayer MoS_2 samples on sapphire substrates were grown in a three temperature-zone chemical vapor deposition

†Corresponding author. E-mail: gyzhang@iphy.ac.cn

© 2022 Chinese Physical Society and IOP Publishing Ltd

(CVD) system. For detailed information on the growth of ML-MoS_2 large single domain, large domain ML-MoS_2 films, and small domain ML-MoS_2, please refer to Refs. [33,35], respectively. For thick MoS_2 flakes, they were mechanically exfoliated from bulk crystals onto scotch-tape, and then transferred onto SiO_2/Si substrates. For the ML-MoS_2 films on SiO_2/Si substrate, the ML-MoS_2 films was etched off substrates by KOH solution and transferred onto the SiO_2/Si substrates.

2.2. Wet etching of the sample

The MoS_2 on substrates were immersed in calcium hypochlorite solution for the desired time. After etching, the sample is rinsed in deionized water to remove chemical residues and terminate the etching process, dried with N_2 gas, and then characterized with optical microscopy.

2.3. Sample characterizations

Raman and PL spectra were carried out by a micro-Raman spectrometer (Horiba LabRAM HR Evolution) in a confocal backscattering configuration with an excitation laser wavelength of 532 nm, a laser power of 1 mW and spot size of 1 μm^2. The PL mapping was obtained with WiTec (Alpha 300R) Raman microscope with a laser power of 1 mW and step size of 1 μm. AFM imaging was performed by Veeco Multimode III under ambient conditions. STEM imaging was performed by an aberration-corrected JEOL Grand ARM 300 CFEG operated at 80 kV.

3. Results

To directly visualize the structural defects in ML-MoS_2, we first use a calcium hypochlorite solution to etch the samples at room temperature grown by CVD. The reaction process of MoS_2 and hypochlorite ion is as follows:[30]

$$MoS_2 + 9ClO^- + 6OH^- \rightarrow MoO_4^{2-} + 9Cl^- + 2SO_4^{2-} + 3H_2O.$$

Since the defects have relatively high chemical reactivity, the etching process starts at the defects first. After the amplification by etching, 0D point defects and 1D grain boundaries transformed into triangular pits and trenches, respectively (Fig. 1(a)). This opens the possibilities to directly observe the structural defects in ML-MoS_2 by an optical microscope. Figure 1(b) shows the typical optical image of a single crystal ML-MoS_2 domain on sapphire substrates after etching with a 2-wt% calcium hypochlorite solution for 20 seconds at room temperature. Obvious pits appeared in the crystal domain after etching. The triangular shape of the etched pits indicating that the etching process has strong anisotropy. Alluringly, the etched triangular pits are in the same direction as the domains. For the CVD grown ML-MoS_2 grown under sulfur-rich conditions, the edges are S-terminated zigzag edges (ZZ_S).[10,31–33] The etched triangular pits in the same direction as the domains should have zigzag edges terminated with molybdenum (ZZ_{Mo}),[24,34] as shown in the inset of Fig. 1(b). Figure 1(c) shows a typical optical image of merged ML-MoS_2 domains on sapphire substrates after etching. It can be seen that the grain boundaries have been etched to be trenches, enable the direct visualization. Figure 1(d) presents the AFM image of the etched trenches, indicating that the edges are very smooth and the surface is clean.

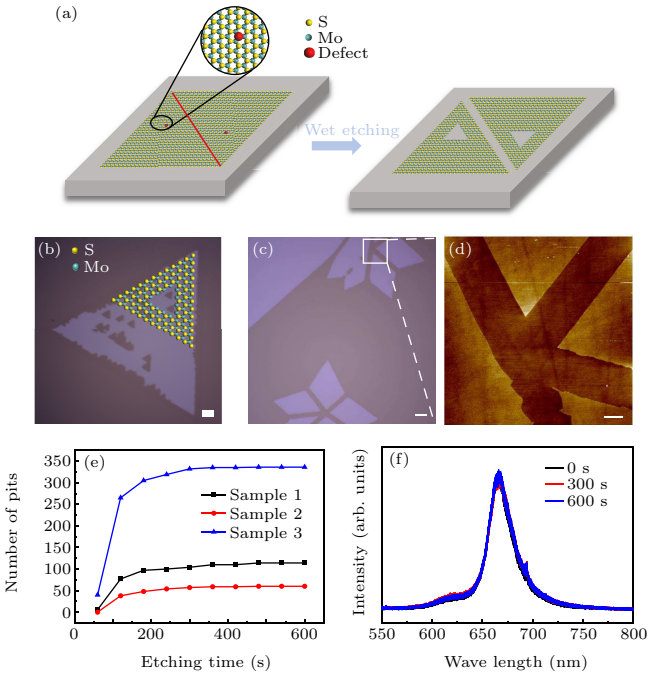


Fig. 1. Anisotropic and non-invasive etching of ML-MoS_2 by calcium hypochlorite solution: (a) schematic diagram of wet etching; (b) optical image of ML-MoS_2 large single domain after etching. The inset shows the schematic diagram of the atomic geometry of ML-MoS_2 large single domain; (c) optical image of merged ML-MoS_2 domains after etching with calcium hypochlorite solution; (d) close-up AFM image of the areas surrounded by lines in panel (c); (e) the evolution of the number of triangular pits in different batches of MoS_2 with the etching time; (f) PL spectra of MoS_2 with different etching times. Scale bar: 10 μm in panels (b) and (c), 1 μm in panel (d).

Figure 1(e) shows the evolution of the number of triangular pits in three triangular domains from different batches with etching time. The number of triangular pits of all the three samples reached saturation after about 200 seconds. This indicates that the etching process of ML-MoS_2 by hypochlorite ion only starts from the inherent defects, and does not generate new defects. This is further confirmed by the perfect atomic structure after etching, please see Fig. S1 for more details. The increase in the number of triangular pits over time in the initial stage of etching may stem from the different chemical reactivity of different defects.[12,13] Figure 1(f) shows that the PL spectra of ML-MoS_2 after etching remained unchanged, even if the etching time was extended to 600 seconds. This indicates that our method is non-invasive and significantly different from previous etching methods.[16,18,21,22] Please see

Fig. S2 for more details of the PL spectra in Supporting information.

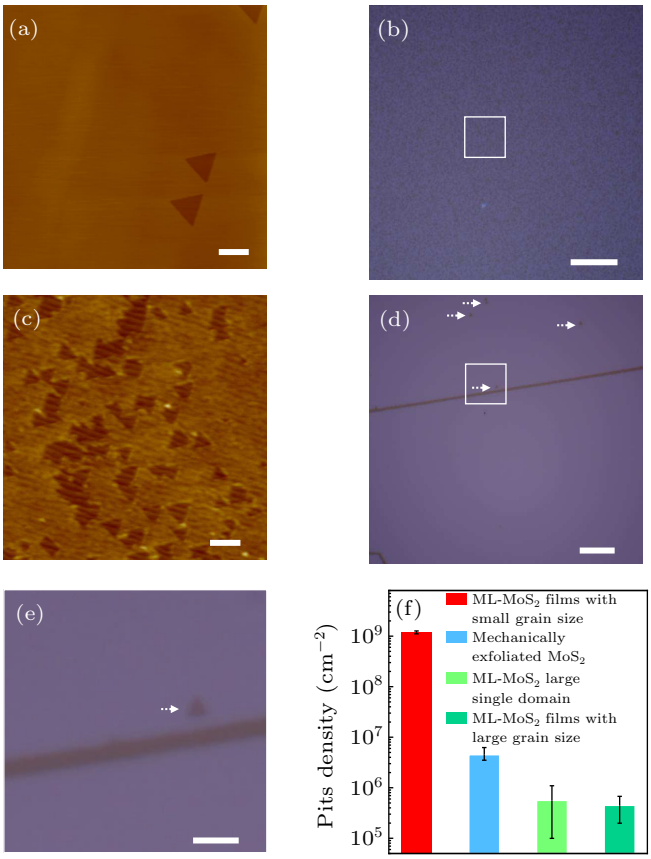


Fig. 2. Defect density of different types of treated MoS_2 samples: (a) AFM image of mechanically exfoliated MoS_2 etched by calcium hypochlorite solution; (b) optical image of CVD-grown ML-MoS_2 films with small grain size etched by calcium hypochlorite solution; (c) close-up AFM image of the areas surrounded by lines in panel (b); (d) optical image of CVD-grown ML-MoS_2 films with large grain size etched by calcium hypochlorite solution. The white arrow points to the location of the triangular pits; (e) close-up optical image of the areas surrounded by lines in panel (d); (f) statistics of average pits densities of various MoS_2 samples. Scale bar: 1 μm in panel (a), 10 μm in panel (b), 300 nm in panel (c), 10 μm in panel (d), 2 μm in panel (e).

Using our non-invasive techniques, we further studied the internal defects of different types of MoS_2, namely, mechanically exfoliated MoS_2, CVD-grown ML-MoS_2 single domain, and CVD-grown ML-MoS_2 films with small and large grain size. After 60 seconds of etching, triangular pits appeared in mechanically exfoliated MoS_2, as shown in Fig. 2(a). The density of triangular pits is $\sim 4.50 \times 10^6$ cm^{-2}. For CVD-grown ML-MoS_2 films with small grain size, as shown in Figs. 2(b) and 2(c), the density of triangular pits is much higher than that of mechanically exfoliated MoS_2 and can reach $\sim 1.18 \times 10^9$ cm^{-2}. Notably, the triangular pits of CVD-grown ML-MoS_2 films with small grain size have two orientations. This is because the film is stitched by two oriented domains: 0° and 60°.[35] For CVD-grown ML-MoS_2 single domain and ML-MoS_2 films with large grain size, the densities of triangular pits are $\sim 4.47 \times 10^5$ cm^{-2} and $\sim 5.61 \times 10^5$ cm^{-2}, respectively, which are much lower than that of CVD-grown ML-MoS_2 films with small grain size and also more than one order of magnitude lower than that of mechanically exfoliated MoS_2. Statistics of average pits densities of various MoS_2 samples are shown in Fig. 2(f). The ultralow defect density in CVD-grown ML-MoS_2 films with large grain size provides key information for understanding the excellent electrical properties recently observed.[33] It is worth noting that in order to avoid the mutual fusion phenomenon of the pits during the etching process, see Fig. S3 for details, the etching time for CVD-grown ML-MoS_2 films with small grain size and mechanically exfoliated MoS_2 is only 60 seconds. This is different from the situations of CVD-grown ML-MoS_2 single domain and ML-MoS_2 films with large grain size where the etching has reached saturation (etching time exceeds 200 seconds). This means that the defect densities in mechanically exfoliated MoS_2 and CVD-grown ML-MoS_2 films with small grain size may be higher than that shown in Fig. 2(f).

Apart from the intrinsic defects, we also use our method to study the artificially introduced defects in MoS_2. Chemical hydrogen plasma treatment can generate sulfur vacancies in MoS_2.[36–38] After treating with calcium hypochlorite solution, MoS_2 treated with hydrogen plasma is quickly etched away. Note that before treating with calcium hypochlorite solution, the structure of MoS_2 treated with hydrogen plasma is intact (Fig. S4). Even if the etching time is shortened to about 0.5 seconds, there are still many pits on the surface of the MoS_2 sample, as shown in Fig. 3(a). The grooves in the image are attributed to the stress caused by the bombardment of hydrogen ions on the MoS_2. This indicates that the calcium hypochlorite solution has a good response to the sulfur vacancies generated by hydrogen plasma. Argon plasma treatment is a physical process and can introduce phase transitions in MoS_2.[39] After argon ion treatment of the CVD-grown ML-MoS_2 films with large grain size, the density of triangular pits is increased by more than three orders of magnitude and can reach 4.70×10^8 cm^{-2}, as shown in Fig. 3(b). Figure S5 shows details about the phase transition. The strongly enhanced defect density in samples treated by argon ion provides new insight to understand the physical mechanism of phase transitions triggered by argon plasma treatment.[40]

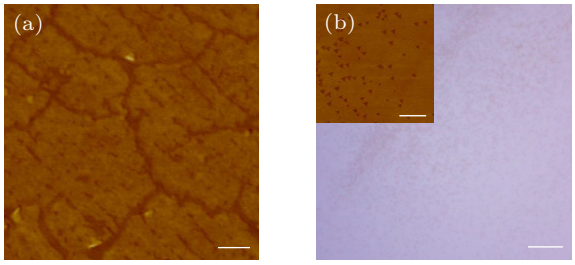


Fig. 3. Response of wet etch to artificial defects: (a) AFM image of MoS_2 treated by hydrogen plasma after being etched by solution; (b) optical image of 1T phase MoS_2 after being etched by solution. The inset is an AFM image of the sample. Scale bar: 100 nm in panel (a), 10 μm in panel (b), 1 μm in the insert of panel (b).

Significantly, the shape of the pit can be highly tunable by the concentration of the solution. As shown in Figs. 4(a)–4(h), as the concentration of calcium hypochlorite solution decreases, the shape of the pits evolves from triangles to truncated triangles, then to hexagons, and finally to inverse triangles. This indicates that the edges of the pit change from pure ZZ_{Mo} to pure ZZ_S as the concentration of the solution decreases.[34] The etch rate of the two types of edge states varies with concentration as shown in Fig. 4(i). In other word, our technique opens up the opportunities to obtain atomically sharp edge states on demand. This provides opportunities for different cut-off boundaries of ML-MoS_2, showing great application potential in metamaterial preparation,[41] heterojunction epitaxy,[42,43] defect repair,[44,45] hydrogen evolution catalysis,[46] nonlinear optics,[47] and nanoelectronics.[48,49] In addition, the anisotropic etching of ML-MoS_2 by the calcium hypochlorite solution is not limited by the substrate. Figure S6 shows that for ML-MoS_2 on SiO_2 substrate, the pits also show triangle sharp, indicating the anisotropy of the etching. In addition to MoS_2, the calcium hypochlorite solution can also be used to etch other 2D-TMDs, such as WSe_2, $MoSe_2$, and WS_2 (Fig. S7). This indicates that our method is a general technique for directly visualizing defects in 2D-TMDs, and has the potential to be applied to other 2D semiconductors.

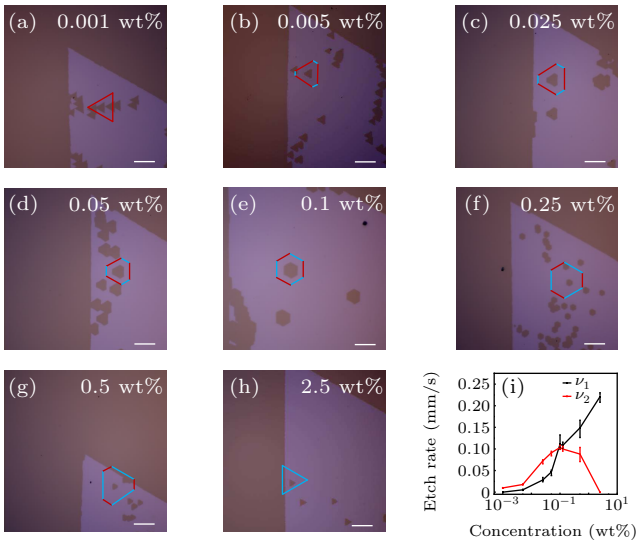


Fig. 4. The shape of the pits etched under different calcium hypochlorite concentrations: (a)–(h) optical images of MoS_2 etched by different concentrations of calcium hypochlorite solutions. The blue and red sides of the triangles and truncated triangles in the illustration correspond to ZZ_{Mo} and ZZ_S, respectively. (i) Etching rate of the two types of boundaries varies with concentration. v_1 and v_2 respectively correspond to the etching rate of Zigzag edges terminated with molybdenum (ZZ_{Mo}) and sulphur (ZZ_S). Scale bar: 10 μm in panels (a)–(h).

4. Summary

In summary, we have developed a simple and non-invasive method to directly visualize the structural defects in 2D-TMDs on a large scale. Utilizing this etching technique, we have investigated the intrinsic defects of four types of MoS_2 samples and found that CVD-grown ML-MoS_2 single domain and ML-MoS_2 films with large grain size have lowest defect density. This enable us to understand the relationship between structural defects and performance. Moreover, for artificially introduced defects, such as sulfur vacancies introduced by hydrogen plasma and phase transition triggered by argon plasma, our method also has a good response. Finally, the edges of by etched pits can be tunable by changing the concentration of the calcium hypochlorite solution, providing the opportunities to obtain edge states on demand.

Acknowledgments

Project supported by the Key-Area Research and Development Program of Guangdong Province, China (Grant No. 2020B0101340001), the Strategic Priority Research Program of Chinese Academy of Sciences (CAS) (Grant No. XDB30000000), and the National Natural Science Foundation of China (Grant Nos. 61888102 and 11834017).

References

[1] Li S L, Tsukagoshi K, Orgiu E and Samori P 2016 *Chem. Soc. Rev.* **45** 118
[2] Zheng J, Du H, Jiang F, Zhang Z, Sa B, He W, Jiao L and Zhan H 2021 *Nano Lett.* **21** 1260
[3] Lee Y H, Zhang X Q, Zhang W J, Chang M T, Lin C T, Chang K D, Yu Y C, Wang J T W, Chang C S, Li L J and Lin T W 2012 *Adv. Mater.* **24** 2320
[4] Liu K K, Zhang W J, Lee Y H, Lin Y C, Chang M T, Su C, Chang C S, Li H, Shi Y M, Zhang H, Lai C S and Li L J 2012 *Nano Lett.* **12** 1538
[5] Ding Z W, Pei Q X, Jiang J W and Zhang Y W 2015 *J. Phys. Chem. C* **119** 16358
[6] McDonnell S, Addou R, Buie C, Wallace R M and Hinkle C L 2014 *ACS Nano* **8** 2880
[7] Voiry D, Salehi M, Silva R, Fujita T, Chen M, Asefa T, Shenoy V B, Eda G and Chhowalla M 2013 *Nano Lett.* **13** 6222
[8] Shi Y, Zhou Y, Yang D R, Xu W X, Wang C, Wang F B, Xu J J, Xia X H and Chen H Y 2017 *J. Am. Chem. Soc.* **139** 15479
[9] Wang X, Zhang Y, Si H, Zhang Q, Wu J, Gao L, Wei X, Sun Y, Liao Q, Zhang Z, Ammarah K, Gu L, Kang Z and Zhang Y 2020 *J. Am. Chem. Soc.* **142** 4298
[10] van der Zande A M, Huang P Y, Chenet D A, Berkelbach T C, You Y, Lee G H, Heinz T F, Reichman D R, Muller D A and Hone J C 2013 *Nat. Mater.* **12** 554
[11] Chen Y, Huang S, Ji X, Adepalli K, Yin K, Ling X, Wang X, Xue J, Dresselhaus M, Kong J and Yildiz B 2018 *ACS Nano* **12** 2569
[12] Hong J, Hu Z, Probert M, Li K, Lv D, Yang X, Gu L, Mao N, Feng Q, Xie L, Zhang J, Wu D, Zhang Z, Jin C, Ji W, Zhang X, Yuan J and Zhang Z 2015 *Nat. Commun.* **6** 6293
[13] Zhou W, Zou X, Najmaei S, Liu Z, Shi Y, Kong J, Lou J, Ajayan P M, Yakobson B I and Idrobo J C 2013 *Nano Lett.* **13** 2615
[14] Lin Y C, Bjorkman T, Komsa H P, Teng P Y, Yeh C H, Huang F S, Lin K H, Jadczak J, Huang Y S, Chiu P W, Krasheninnikov A V and Suenaga K 2015 *Nat. Commun.* **6** 6736
[15] Addou R, Colombo L and Wallace R M 2015 *ACS Appl. Mater. Interfaces* **7** 11921
[16] Yamamoto M, Einstein T L, Fuhrer M S and Cullen W G 2013 *J. Phys. Chem. C* **117** 25643
[17] Ryu Y, Kim W, Koo S, Kang H, Watanabe K, Taniguchi T and Ryu S 2017 *Nano Lett.* **17** 7267
[18] Zhou H, Yu F, Liu Y, Zou X, Cong C, Qiu C, Yu T, Yan Z, Shen X, Sun L, Yakobson B I and Tour J M 2013 *Nano Res.* **6** 703
[19] Jeong H Y, Lee S Y, Ly T H, Han G H, Kim H, Nam H, Jiong Z, Shin B G, Yun S J, Kim J, Kim U J, Hwang S and Lee Y H 2016 *ACS Nano* **10** 770

[20] Shi Y, Huang J K, Jin L, Hsu Y T, Yu S F, Li L J and Yang H Y 2013 *Sci. Rep.* **3** 1839
[21] Ye G, Gong Y, Lin J, Li B, He Y, Pantelides S T, Zhou W, Vajtai R and Ajayan P M 2016 *Nano Lett.* **16** 1097
[22] Xu C Y, Qin J K, Yan H, Li Y, Shao W Z and Zhen L 2018 *Appl. Surf. Sci.* **452** 451
[23] Wu S, Yang R, Shi D and Zhang G 2012 *Nanoscale* **4** 2005
[24] Li J, Hu S, Chen Z, Liang Y, Kang H, Zhang Y, Sui Y, Wang S, Yu G, Peng S, Jin Z and Liu X 2020 *Appl. Surf. Sci.* **510** 145412
[25] Wang Z, Li Q, Xu H, Dahl-Petersen C, Yang Q, Cheng D, Cao D, Besenbacher F, Lauritsen J V, Helveg S and Dong M 2018 *Nano Energy* **49** 634
[26] Wang J, Xu X, Qiao R, Liang J, Liu C, Zheng B, Liu L, Gao P, Jiao Q, Yu D, Zhao Y and Liu K 2018 *Nano Res.* **11** 4082
[27] Kim K, Lee H B, Johnson R W, Tanskanen J T, Liu N, Kim M G, Pang C, Ahn C, Bent S F and Bao Z 2014 *Nat. Commun.* **5** 4781
[28] Yu S U, Park B, Cho Y, Hyun S, Kim J K and Kim K S 2014 *ACS Nano* **8** 8662
[29] Ago H, Fukamachi S, Endo H, Solis-Fernandez P, Yunus R M, Uchida Y, Panchal V, Kazakova O and Tsuji M 2016 *ACS Nano* **10** 3233
[30] Warren I H and Mounsey D M 1983 *Hydrometallurgy* **10** 343
[31] Wan W, Zhan L J, Xu B B, Zhao F, Zhu Z W, Zhou Y H, Yang Z L, Shih T and Cai W W 2017 *Small* **13** 1603549
[32] Yu H, Yang Z, Du L, Zhang J, Shi J, Chen W, Chen P, Liao M, Zhao J, Meng J, Wang G, Zhu J, Yang R, Shi D, Gu L and Zhang G 2017 *Small* **13** 1603005
[33] Wang Q Q, Li N, Tang J, Zhu J Q, Zhang Q H, Jia Q, Lu Y, Wei Z, Yu H, Zhao Y C, Guo Y T, Gu L, Sun G, Yang W, Yang R, Shi D X and Zhang G Y 2020 *Nano Lett.* **20** 7193
[34] Stehle Y Y, Sang X, Unocic R R, Voylov D, Jackson R K, Smirnov S and Vlassiouk I 2017 *Nano Lett.* **17** 7306
[35] Yu H, Liao M Z, Zhao W J, Liu G D, Zhou X J, Wei Z, Xu X Z, Liu K H, Hu Z H, Deng K, Zhou S Y, Shi J A, Gu L, Shen C, Zhang T T, Du L J, Xie L, Zhu J Q, Chen W, Yang R, Shi D X and Zhang G Y 2017 *ACS Nano* **11** 12001
[36] Lee J Y, Kim J H, Jung Y, Shin J C, Lee Y, Kim K, Kim N, van der Zande A M, Son J and Lee G H 2021 *Commun. Mater.* **2** 80
[37] Cheng C C, Lu A Y, Tseng C C, Yang X L, Hedhili M N, Chen M C, Wei K H and Li L J 2016 *Nano Energy* **30** 846
[38] Lu A Y, Zhu H, Xiao J, Chuu C P, Han Y, Chiu M H, Cheng C C, Yang C W, Wei K H, Yang Y, Wang Y, Sokaras D, Nordlund D, Yang P, Muller D A, Chou M Y, Zhang X and Li L J 2017 *Nat. Nanotechnol.* **12** 744
[39] Zhu J Q, Wang Z C, Yu H, Li N, Zhang J, Meng J L, Liao M Z, Zhao J, Lu X B, Du L J, Yang R, Shi D, Jiang Y and Zhang G Y 2017 *J. Am. Chem. Soc.* **139** 10216
[40] Shi S, Sun Z and Hu Y H 2018 *J. Mater. Chem. A* **6** 23932
[41] Munkhbat B, Yankovich A B, Baranov D G, Verre R, Olsson E and Shegai T O 2020 *Nat. Commun.* **11** 4604
[42] Li M Y, Shi Y M, Cheng C C, Lu L S, Lin Y C, Tang H L, Tsai M L, Chu C W, Wei K H, He J H, Chang W H, Suenaga K and Li L J 2015 *Science* **349** 524
[43] Zhang Z W, Chen P, Duan X D, Zang K T, Luo J and Duan X F 2017 *Science* **357** 788
[44] Li X, Dong J, Idrobo J C, Puretzky A A, Rouleau C M, Geohegan D B, Ding F and Xiao K 2017 *J. Am. Chem. Soc.* **139** 482
[45] Ma T, Ren W C, Liu Z B, Huang L, Ma L P, Ma X L, Zhang Z Y, Peng L M and Cheng H M 2014 *ACS Nano* **8** 12806
[46] Jaramillo T F, Jorgensen K P, Bonde J, Nielsen J H, Horch S and Chorkendorff I 2007 *Science* **317** 100
[47] Yin X, Ye Z, Chenet D A, Ye Y, O'Brien K, Hone J C and Zhang X 2014 *Science* **344** 488
[48] Li Y F, Zhou Z, Zhang S B and Chen Z F 2008 *J. Am. Chem. Soc.* **130** 16739
[49] Bollinger M V, Lauritsen J V, Jacobsen K W, Norskov J K, Helveg S and Besenbacher F 2001 *Phys. Rev. Lett.* **87** 196803